ISSN1027-5495. Functional Materials, 31, No.1 (2024), p. 18-25
doi:http://dx.doi.org/10.15407/fm31.01.18

Crystallization of amorphous Sb_2Se_3 films according to TEM with *in situ* video recording

A.G. Bagmut

National Technical University "Kharkiv polytechnic institute",
2 Kyrpychova St., 61002 Kharkiv, Ukraine

Received December 12, 2023

The structure and kinetics of the crystallization process in amorphous Sb_2Se_3 films were studied using electron diffraction and transmission electron microscopy (TEM) with *in situ* video recording. It is found that under the action of electron irradiation, the film crystallizes in an island polymorphous mode with a *relative length* $\delta_0 \sim 200$. Direct electron microscopic observations have shown that new nuclei appear at each stage of growth and so-called *continuous nucleation* occurs. Time dependence of the volume fraction of crystallized particles is exponential, described by the Johnson-Mehl-Avrami-Kolmogorov (JMAK) equation. The closest integer value of the Avrami exponent is $n = 2$.

Keywords: amorphous state, kinetics, Sb_2Se_3, crystallization; electron microscopy, videorecording.

Кристалізація аморфних плівок Sb_2Se_3 за ПЕМ з відеозаписом "*in situ*". *О.Г. Багмут*

Структура і кінетика кристалізаційних процесів в аморфних плівках Sb_2Se_3 досліджена за допомогою електронної дифракції і просвічувальної електронної мікроскопії (ПЕМ) з відеорегістрацією "*in situ*". Встановлено, що під дією електронного випромінювання в плівці спостерігається острівцева поліморфна кристалізація з відносною довжиною $\delta_0 \sim 200$. Прямі електронно-мікроскопічні спостереження показали, що на кожному етапі перетворення з'являються нові зародки і має місце так звана " *безперервна нуклеація*" ("continuous nucleation"). Залежність частки кристалічної фази від часу носить експоненційний характер, що описується рівнянням Johnson-Mehl-Avrami-Kolmogorov (JMAK). Найближче ціле значення показника Аврамі $n = 2$.

1. Introduction

Materials in the non-crystalline (amorphous) solid state are used in almost all areas of electronic instrumentation. The reliable and trouble-free operation of electronic devices is directly dependent on the stability of the amorphous structure of the substances that make up the elements of the electronic device. However, for most materials the amorphous state is metastable. Hence, amorphous films can crystallize spontaneously or due to physical actions, i.e., transition to a more stable crystalline state. Crystallization of an amorphous substance is a first-order phase transition. One of its types is polymorphous crystallization, whereby a substance converts from an amorphous into a crystalline state without changing its composition. This is typical for both pure elements and stoichiometric chemical compounds.

Spontaneous polymorphous crystallization of an amorphous layer (natural aging) can take a long time (years and decades). This complicates predicting the reliability and durability of the electronic device. However, it is possible to comprehensively study the structural transition of a substance from an amorphous to a crystalline state outside the device. Modeling of crystallization can be done inside a transmis-

sion electron microscope (TEM). In a certain operating mode of the microscope, an electron beam can initiate the crystallization of an object with an amorphous structure. In this case, the film crystallization can be observed visually ("in situ" method). The combination of various TEM operating modes provides comprehensive information on the structural, morphological, and kinetic parameters of the crystallization process.

The kinetics of the phase transition from amorphous to the crystalline state (*a-c* transition) in most cases is adequately described with the classic Johnson-Mehl-Avrami-Kolmogorov (JMAK) theory through the equation:

$$x(t) = 1 - \exp(-kt^n), \quad (1)$$

where x is the transformed volume fraction, t is time, k is the effective rate, and n is the Avrami exponent [1, 2]. The graph of ln[-ln(1-x)] versus ln(t) should be a straight line:

$$\ln[-\ln(1-x)] = n\ln t + \ln k. \quad (2)$$

According to (2), n is the tangent of the inclination angle of the line to the abscissa, and ln$k$ is the point of the intersection with the ordinate.

If the thickness of the amorphous film is small, the *a-c* process is well described within the unlimited two-dimensional space. In this case, crystallization is called *site saturation,* if all the nuclei present in the amorphous medium begin to grow at the beginning of the *a-c* transformation [2]. According to JMAK theory, in this case the Avrami exponent is n =2. This situation was realized in experiments on electron-beam crystallization of amorphous ZrO_2 films deposited by laser evaporation. Values n = 1.3, 1.8, 2.0 are noted for different tangential crystal growth rates [3]. In contrast to site saturation, when new nuclei appear at every step of the transformation, n =3, and the process is called *continuous nucleation* [2]. This situation was realized in experiments on electron-beam crystallization of amorphous Yb_2O_2S (n = 1.8), Ta_2O_5 (n = 1.7), V_2O_3 (n = 1.8) films [4 - 6].

Along with the exponential dependence (1), there is also a quadratic dependence $x(t) \sim t^2$. This is the case of the electron-beam crystallization of amorphous of Cr_2O_3 [7], Sb_2S_3 [8], and $Ti_{41}Zr_{41}Ni_{18}$ films [9]. The classification of these pathways, carried out according to the most appropriate parameters, provides both qualitative and quantitative systematization of the phase transformation. As applied to thin amorphous films that crystallize under the influence of electron irradiation, the relevant parameters are structural and morphological characteristics. These are the size, shape, structure, orientation, and numerical density of crystalline nuclei growing in an amorphous medium. They make it possible to attribute the reaction qualitatively to one or another crystallization mode [10]. The relative length δ_0 considered in [10, 11] can serve as a quantitative characteristic of the crystallization mode. This is a dimensionless number equal to the ratio of the characteristic unit of length to the value of the geometric parameter of the elementary cell of the crystal. The relative length δ_0 was determined as [4, 11]:

$$\delta_0 = \frac{D_0}{\sqrt[3]{\Omega}}, \quad (3)$$

where characteristic unit of length D_0 is the crystal size at time t_0, after which the volume of the amorphous phase decreases by a factor of e = 2.718. Ω is the volume of the unit cell of a growing crystal.

In the case of island polymorphous crystallization (IPC), numerous misoriented crystals grow in the amorphous film in the region of electron beam action. The transformed volume fraction x is described by the equation (1), and δ_0 is about several hundred. Unlike IPC, in layer polymorphous crystallization (LPC), one crystal grows in an amorphous film in the region of electron beam action. The transformed volume fraction $x(t) \sim t^2$ and δ_0 is about several thousand [10]. Determination of δ_0 is possible using the electron microscopic method "in situ" and video recording of the fast crystallization process.

The kinetics of electron-beam crystallization of amorphous Sb_2Se_3 films is studied in this work. Sb_2Se_3 belongs to the narrow-gap semiconductors of the V_2VI_3 group and has a structure similar to Sb_2S_3 [12, 13]. The compound has an orthorhombic lattice with parameters a = 1.163 nm, b = 1.178 nm, c = 0.3985 nm [13]. This photoelectric absorbing material is promising due to its high electro-optical properties [14-17] and can be used for the creation of thin-film solar cells [15, 16]. It was reported that during annealing of Sb_2Se_3, the *a-c* phase transition occurs at 423 K [12].

The purpose of this work is to determine the kinetic and structural-morphological characteristics of the crystallization of amorphous Sb_2Se_3 in a thin-film state and classify the a-c transformations.

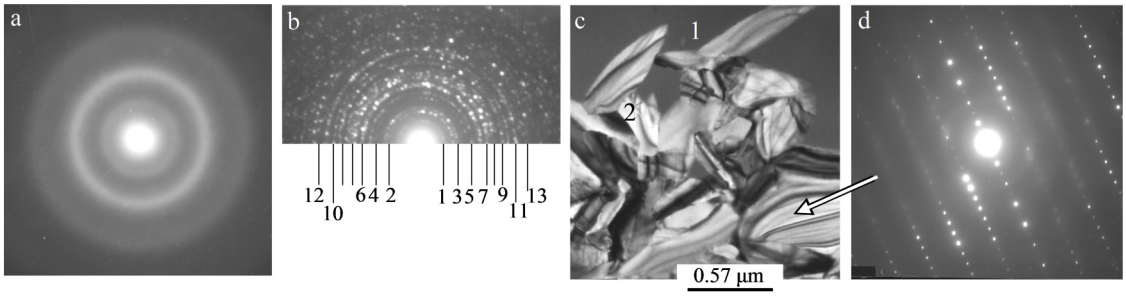

Fig. 1. Crystallization of an amorphous Sb_2Se_3 film: a - electron diffraction pattern in the initial state; b - the same after partial crystallization by the electron beam; c - TEM image of the partially crystallized film (1-amorphous phase, 2-crystalline phase); d - SAED pattern from one of the Sb_2Se_3 grains.

2. Experimental

The samples were free-standing amorphous Sb_2Se_3 films with a thickness h = 30 nm, obtained by thermal evaporation in vacuum. According to [8], amorphous Sb_2Se_3 films were grown on the (001) face of KCl single crystals at room temperature by thermal evaporation of a sample in a vacuum chamber (~10^{-6} Torr). Evaporation occurs during rapid heating a tantalum crucible by passing an electric current pulse. Films were separated from the substrate in distilled water and transferred onto subject grids for electron microscopy studies. Homogeneous areas of amorphous film with a uniform electron-microscopic thickness contrast were studied. The composition stoichiometry was controlled by the nature of crystallization and the selected area electron diffraction (SAED) patterns of the crystallized sections of the film.

Features of the *a-c* phase transformation were studied by electron diffraction and transmission electron microscopy (TEM) at an accelerating voltage of 100 kV. The crystallisation was initiated by the electron beam inside the electron microscope column. This made it possible to register the structural transformations "in situ". The radiation dose rate was estimated from the beam current and the diameter of the electron beam focused at the sample. At a current of 20 μA and a diameter of 5 μm the radiation dose rate was ~ $6 \cdot 10^4$ $e^-/Å^2 \cdot s$.

A Canon Power Shot G15 camera at the frame rate of 30 s^{-1} was used for video recording of the crystallization process. Based on the obtained film images, kinetic crystallization curves $x = x(t)$ were constructed. Electron microscopic visualization of crystals in an amorphous matrix was carried out in the bright field mode due to the different nature of the contrast of the amorphous (thickness contrast) and crystalline (diffraction contrast) phases. The Sb_2Se_3 crystals in the reflective position appeared dark against the gray background of the amorphous matrix, while the crystals in the non-reflective position looked light against the gray background of the amorphous matrix. The total area occupied by the crystals was measured in an electron microscopic image of the analyzed section of the film. The content of the crystalline fraction x in the video image was defined according to [9] as the ratio

$$x = \frac{S(t)}{S_f}, \tag{4}$$

where $S(t)$ is the area occupied by the crystalline phase in the image at an arbitrary time moment t and S_f is the area of the field under study. The crystal diameter $D(t)$ at time t was determined from the relation

$$D(t) = \sqrt{\frac{4S_k(t)}{\pi}}, \tag{5}$$

where $S_k(t)$ is the area of the crystal image at time t. The average size of the crystals:

$$\langle D \rangle = \frac{1}{N}\sum_{1}^{N} D_i, \tag{6}$$

where D_i is the diameter of an i-th single crystal.

3. Results and discussion

In the initial state, the Sb_2Se_3 film deposited on the substrate at room temperature was amorphous. This is evidenced by three diffuse halos in the electron diffraction pattern (Fig. 1a). The second halo is intense, while the first and third ones are much weaker in the intensity and very diffuse. The positions of the maxima of the first, second and third diffuse halos correspond to interplanar distances of 0.5, 0.3 and 0.2 nm of the object under study respectively.

Fig. 1b shows the electron diffraction pattern of the same film after its partial electron beam crystallization. The film is two-phase containing amorphous and polycrystalline

Table 1. Results of the decoding of the electron diffraction pattern in Fig.1b

Diffraction ring number	This work d (nm)	hkl	Data [12] d (nm)	Data [13] d (nm)
1	0.826	110	0.828473	0.8280
2	0.585	020	0.589384	0.5890
3	0.521	120	0.526006	0.5250
4	0.416	220	0.414212	0.414
5	0.369	310	0.368730	0.3682
6	0.316	211	0.316357	0.3162
7	0.282	221	0.286798	0.2868
8	0.252	321	-	0.2513
9	0.228	510	-	0.2282
10	0.213	520	0.216460	0.2164
11	0.198	002	0.198935	0.1989
12	0.195	600	0.193782	0.1938
13	0.171	360	-	0.1752

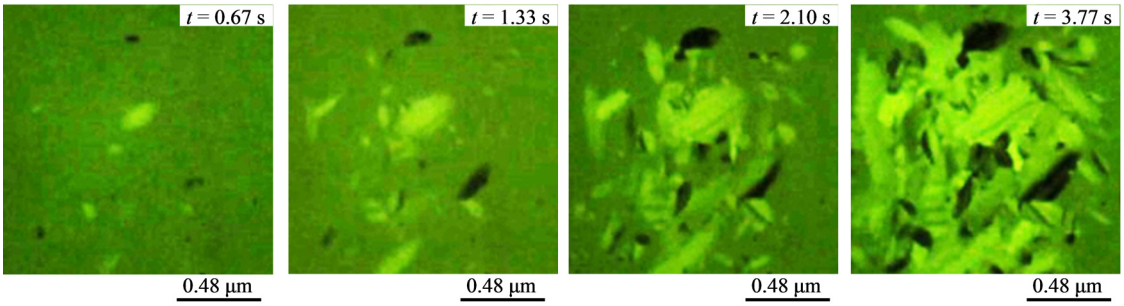

Fig. 2. Video frames of crystal growth in amorphous Sb_2Se_3 films under electron beam irradiation. Time periods t from the beginning of recording the crystallization process are shown in the upper right corner of each frame.

components. The TEM image of the partially crystallized film (1-amorphous phase, 2-crystalline phase) and SAED pattern from one of the Sb_2Se_3 grains are presented in Figs. 1c and 1d respectively.

The results of the decoding the electron diffraction pattern presented at Fig. 1b are summarized in Table 1. The correspondence between experimental and literature data [12, 13] was observed. The absence of reflections associated with Sb and Se indicates the one-stage polymorphous *a-c* transformation in Sb_2Se_3.

Fig. 2 shows video images of crystals grown in an amorphous Sb_2Se_3 film. Based on the frame-by-frame analysis of this video, the dependences of the crystal concentration N on time t were obtained. At a fixed electron dose rate, N increases linearly with time. The dependence $N(t)$ is shown in Fig. 3a. The straight line corresponds to the equation:

$$N = 7.41 \cdot 10^8 t + 1.63 \cdot 10^7 \text{ cm}^{-2}, \qquad (7)$$

where t is measured in seconds. According to (7), the nucleation rate is $\alpha = 7.41 \cdot 10^8 \text{ cm}^{-2}\text{s}^{-1}$.

The time dependences of the average crystal diameter $\langle D \rangle$ and the maximum crystal diameter D_{max} are shown in Fig. 3b by the lines 1 and 2 respectively. The straight lines correspond to the equations:

$$\langle D \rangle = 0.0519t + 0.0371 \text{ μm}, \qquad (8a)$$

$$D_{max} = 0.1734t + 0.0564 \text{ μm}. \qquad (8b)$$

According to (8a), the average tangential crystal growth rate is $\langle v_\tau \rangle = 0.0519 \text{ μm} \cdot \text{s}^{-1}$ and the maximum tangential crystal growth rate according to (8b) is $v_{\tau max} = 0.1734 \text{ μm} \cdot \text{s}^{-1}$. Thus, the average crystal growth rate is more than three times less than the maximum. The data on α, $\langle v_\tau \rangle$ and $v_{\tau max}$ are given in Table 2.

The distributions of crystal sizes D in the amorphous Sb_2Se_3 film at times $t = 0.67$ s (Fig. 1a) and $t = 1.33$ s (Fig.1b) after the beginning of recording the *a-c* process are shown in Fig. 4a and 4b respectively. The given histograms indicate the presence of asymmetry and kurtosis in the distributions. At $t = 0.67$ s the asymmetry coefficient is 2.08 and the kurtosis is 6.50,

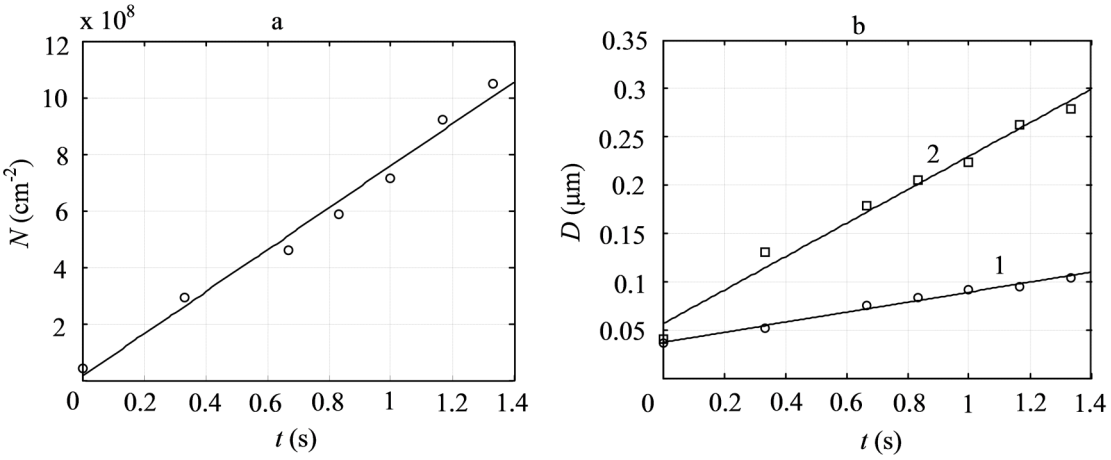

Fig. 3. Time dependences of the numerical density N of crystals (a) and their diameters D (b) in amorphous Sb_2Se_3 film: 1– average diameter $<D>$; 2-maximum diameter D_{max}

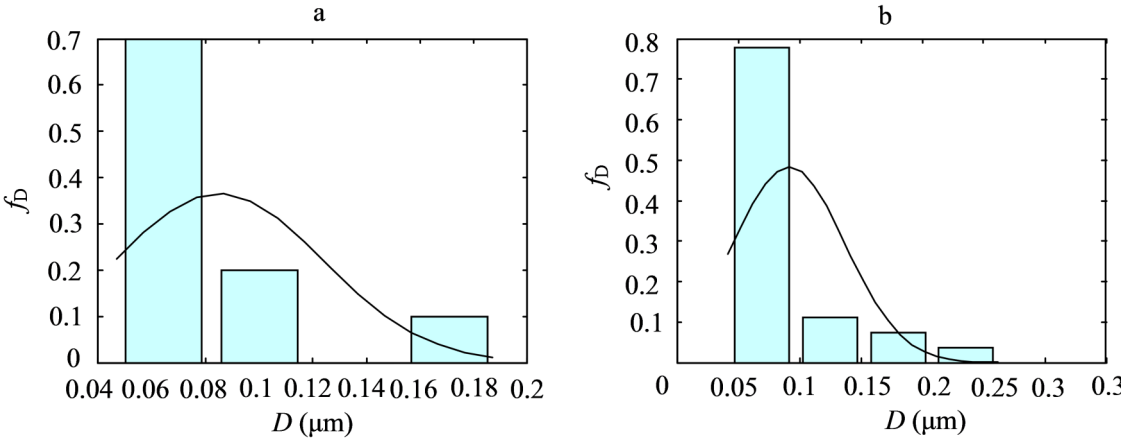

Fig. 4. Histograms of relative frequencies f_D of crystal diameters D in an amorphous of Sb_2Se_3 film at times t = 0.67 s (a) and t = 1.33 s (b) after beginning of recording the a-c process, and the curve corresponding to the Gaussian distribution.

$<D>$ = 0.085 μm. Similar data for the distribution at t = 1.33 s are: asymmetry coefficient is 2.19, kurtosis is 8.60 and $<D>$ = 0.091 μm.

The time dependence of the crystallized volume fraction $x(t)$ is shown in Fig. 5a. These experimental data, presented in the coordinates $\ln[-\ln(1-x)]$ $-\ln t$, form a straight line (Fig. 5b). This fact indicates the applicability of the JMAK formulas (1) and (2) to the process of a-c phase transformation.

According to (2) and Fig. 5b, n = 2.16, $\ln k$ = – 2.44 and k = 0.08733 s^{-2}. The case α = const and $<v_\tau>$ = const corresponds to the α-version of Kolmogorov's model [18]. This is the case of the continuous nucleation, when the system keeps adding nuclei with the same rate over the entire transformation period [2]. Data on n and k are given in Table 2.

Taking into account numerical values of n and k, the curve in Fig. 5a will fit the equation:

$$x_1 = 1 - \exp(-0.08733t^{2.16}) \qquad (9)$$

If during the a-c transformation, the amorphous phase fraction decreases by a factor of e = 2.72, then the crystalline phase fraction is x = 0.632. When the crystalline phase fraction is x = 0.632 in the film, the characteristic time t_0 = 3.09 s according to (9). For this value, according to (8a), the characteristic length is $D_0 \approx$ 0.16 μm. For Sb_2Se_3, the unit cell volume is $\Omega = 546.09 \cdot 10^{-12}$ μm^3 [13]. In this case, according to (3), the relative length is $\delta_0 \approx 196$. All of them are listed in Table 2.

The passage of electrons through the film causes its Joule-Lenz heating (excitation of phonons) and can create radiation damage. For

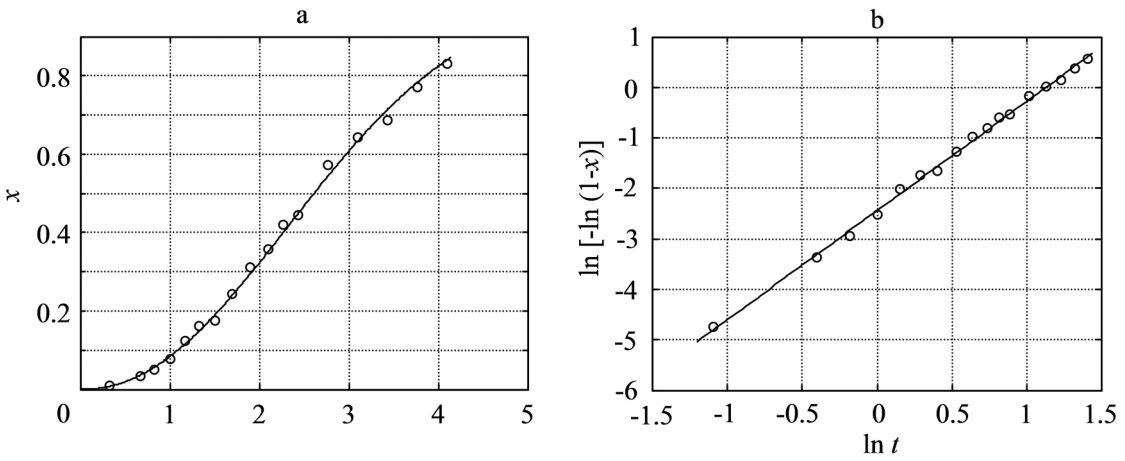

Fig. 5. Time dependence of the crystallized volume fraction $x(t)$ in amorphous Sb_2Se_3 film in coordinates x - t (a) and in coordinates ln[-ln(1-x)] – ln t (b)

excitation of phonons, energy of ~ 0.01 eV is sufficient [21]. Therefore, heating of the film is always present to one degree or another. When using accelerating voltage of 100 - 125 kV and a current of 50 - 75 μA without a condenser diaphragm and with appropriate beam focusing at the object, it is possible to obtain a high temperature, sufficient not only for crystallization of amorphous Fe-C films [22], but also for the melting of refractory materials, such as carbon [23]).

An important damage to unstable and organic substances is ionization, which leads to the chemical decomposition of a substance under the influence of an electron beam. Elementary radiation action is the direct knocking out of atoms from their positions and the formation of primary point defects. Their coagulation (at the appropriate temperature) can initiate the crystallization of an amorphous substance resistant to chemical decomposition.

To create radiation damage, an electron must transfer to the atom an energy E_T exceeding the threshold displacement energy E_D (23 – 51 eV [24]). With an accelerating voltage of 100 kV, the electron energy is E = 100 keV. The masses of the atoms, that make up the film under study, are M_{Sb}~$2.02 \cdot 10^{-25}$ kg, M_{Se}~$1.24 \cdot 10^{-25}$ kg. According to the relation [24]

$$E_T = 2E \cdot (E+2m_0c^2)\, M^{-1}c^{-2}, \qquad (10)$$

where m_0 is the electron rest mass, M is the mass of the atom and c is the speed of light, we get $E_T \approx 2$ eV for the Sb atom and $E_T \approx 3$ eV for the Se atom. This is not enough to create significant radiation damage in the studied film.

Therefore, we believe that the main reason for the crystallization of an amorphous film in our case is Joule-Lenz heating of the film due to phonon excitation by electrons.

Previous studies of amorphous Cr_2O_3 films obtained by laser sputtering of chromium in an oxygen atmosphere have shown that there are no significant differences between the electron-beam induced and heat-induced crystallization. The impact of an electron beam (E = 100 keV) on an amorphous free-standing film initiated the growth of a rounded and crescent-shaped Cr_2O_3 crystals with a hexagonal lattice [25]. A similar structure and morphology of Cr_2O_3 crystals was observed during thermal annealing of an amorphous free-standing film in a muffle furnace for five minutes at a temperature of 400°C

Table 2. Parameters of the electron beam induced crystallization of amorphous Sb_2Se_3 films *

h (nm)	30
$\langle v_\tau \rangle$ (μm/s)	0.0519
$v_{\tau max}$ (μm/s)	0.1734
t_0 (s)	3.09
D_0 (μm)	0.16
n	2.16
k (s^{-2})	0.08733
α ($cm^{-2} \cdot s^{-1}$)	$7.41 \cdot 10^8$
δ_0	196

*h is the thickness of the film, $\langle v_\tau \rangle$ is the average tangential growth rate of the crystals, $v_{\tau max}$ is the maximum tangential crystal growth rate, t_0 is the characteristic time, D_0 is the characteristic length, n is the Avrami exponent, k is the rate constant, α is the nucleation rate, δ_0 is the relative length.

[26]. A strong diffraction contrast of extinction bend contours (depicting the regions where Bragg's law is satisfied) caused by a change in the density of the substance during crystallization was observed. The only difference was in the distribution of crystals over the area of the film. During thermal initiation, crystals grew over the entire area of the film; while during electron beam initiation, they grew only in the region of the electron beam impact. The dominant role of the heat-induced crystallization of amorphous *a*-GeAu films under the action of an electron beam also was noted in [27].

4. Conclusions

During vacuum thermal evaporation of a powder sample, an antimony selenide amorphous film is formed on the substrate at a room temperature. Electron irradiation of the free-standing amorphous film with a dose rate ~ $6 \cdot 10^4$ $e^-/Å^2 \cdot s$ inside the column of the electron microscope causes its crystallization due to Joule-Lenz heating. In situ electron microscopy studies with the video recording method demonstrated that the *a-c* phase transformation occurs in the island polymorphous crystallization mode with the relative length $\delta_0 \approx 196$.

The time dependence of the crystallized volume fraction $x(t)$ in amorphous Sb_2Se_3 film has an exponential character described by the JMAK formula. The polycrystalline film forms at the constant crystal growth rate and constant nucleation rate corresponding to the α-version of the Kolmogorov model (continuous nucleation process). The Avrami exponent is $n = 2.16$ (the nearest integer is 2). These values of n are typical for the crystallization process in which the grain growth occurs with nucleation. Values n with the nearest integer 2 correspond to the crystallization of thin amorphous films of $Ge_1Sb_2Te_4$ [19], Ta_2O_5 [20], Yb_2O_2S [4], V_2O_3 [6].

Acknowledgment

The authors are grateful to A.Yu. Sipatov and N.A. Reznik for the helpful discussions and assistance in sample preparation and research; and M.A. Sokol for assistance in the design of the article.

References

1. J. Ocenasek, P. Novak, S. Agbo, *J. Appl. Phys.*, **115**, 043505-1, (2014). https://doi.org/10.1063/1.4862858
2. M. Castro, F. Domınguez-Adame, A. Sanchez, T. Rodrıguez, *Appl. Phys. Lett.*, **75**, 2205 (1999). https://doi.org/10.1063/1.124965
3. A. Bagmut, V. Beresnev, *Phys. Solid State*, **59**, 151 (2017). https://link.springer.com/article/10.1134/S1063783417010024
4. A. Bagmut, I. Bagmut, *J. Non-Cryst. Solids*, **547**, 120286 (2020). https://doi.org/10.1016/j.jnoncrysol.2020.120286
5. A. Bagmut, *Funct. Mater.*, **29**, 52 (2022). https://doi.org/10.15407/fm29.01.52
6. A.G. Bagmut, Phys. Solid State. 59 1225 (2017). https://doi.org/10.1134/S1063783417060038.
7. A. Bagmut, *J. Cryst. Growth*, **492**, 92 (2018). https://doi.org/10.1016/j.jcrysgro.2018.03.038
8. A.G. Bagmut, *Funct. Mater.*, **28**, 444 (2021). https://doi.org/10.15407/fm28.03.444
9. A. Bagmut, I. Bagmut, A. Devizenko, Eur. Phys. *J. Appl. Phys.*, **98**, 1 (2023). https://doi.org/10.1051/epjap/2023220293
10. A. Bagmut, *Problems of Atomic Science and Technology*, **137**(1), 64 (2022). https://doi.org/10.46813/2022-137-064
11. A. Bagmut, *Funct. Mater.*, **26**, 6 (2019). https://doi.org/10.15407/fm26.01.6.
12. E.A. El-Sayad, A.M. Moustafa, S.Y. Marzouk, *Physica B*, **404** 1119 (2009). https://doi.org/10.1016/j.physb.2008.11.086
13. JCPDS Powder Diffraction File Card No. 15-0861 (International Centre for Diffraction Data, Swarthmore, PA, 1996).
14. P. Sun, Z. Wu, C. Ai et. al., ChemistrySelect, 1, 1824 (2016) https://doi.org/10.1002/slct.201600289
15. Chao Chen, Weiqi Li, Ying Zhou et. al., *Appl. Phys. Lett*. **107**, 043905 (2015). https://doi.org/10.1063/1.4927741
16. Chao Chen, Xinxing Liu, Kanghua Li et. al., *Appl. Phys. Lett*. **118**, 172103 (2021). https://doi.org/10.1063/5.0030430
17. M.-Z. Xue, Z.-W. Fu, *J. Alloys Compounds*, **458**, 351 (2008). https://doi.org/10.1016/j.jallcom.2007.03.109
18. A.N Kolmogorov, Bull. of the Acad. of Sciences of the USSR, *Mathematics Series*, **1**, 355 (1937). https://www.scirp.org/(S(i43dyn45teexjx455qlt3d2q))/reference/ReferencesPapers.aspx?ReferenceID=880675
19. N. Ohshima, *J. Appl. Phys.*, **79** 8357 (1996) https://doi.org/10.1063/1.362548
20. K.-H. Min, R. Sinclair, I.-S. Park et. al., *Phil. Mag.*, **85**, 2049 (2005) https://doi.org/10.1080/14786430500036546

21. L.W. Hobbs, Radiation effects in analysis of inorganic specimens by TEM, in: J. J. Hren, J. I. Goldstein, D. C. Joy (Eds.), Introduction to Analytical Electron Microscopy, Plenum, New York, 1979, pp. 437 - 490. https://link.springer.com/chapter/10.1007/978-1-4757-5581-7_17
22. S.M. Zharkov, L.I. Kveglis, *Phys. Solid State*, **46**, 969 (2004) https://link.springer.com/article/10.1134/1.1744977
23. H König, *Naturwissenschaften* **34**, 108 (1947). https://doi.org/10.1007/BF00602631
24. M.W. Thompson. Defects and Radiation Damage in Metals, London: Cambridge U.P., 1969 https://catalogue.nla.gov.au/Record/2506345
25. A.G. Bagmut, V.A. Zhuchkov, D.V. Melnichenko, *Functional Materials* **14**, 351 (2007).
26. V.Yu. Kolosov, K.L. Shvamm, A.G. Bagmut, S.N. Grigorov, Journal of Surface Investigation: X-ray, Synchrotron and Neutron Techniques 10, 100 (2004) [In Russian].
27. Long Ba and Yong Qin, *J. Appl. Phys*. **80**, 6170 (1996). https://doi.org/10.1063/1.363691